Available online at www.sciencedirect.com
ScienceDirect
Trans. Nonferrous Met. Soc. China 23(2013) 3249−3256
Transactions of Nonferrous Metals Society of China
www.tnmsc.cn

Microstructure evolution of laser deposited Ti60A titanium alloy during cyclic thermal exposure

A-li ZHANG, Dong LIU, Hai-bo TANG, Hua-ming WANG

Engineering Research Center of Ministry of Education on Laser Direct Manufacturing for Large Metallic Components, Beihang University, Beijing 100191, China

Received 26 October 2012; accepted 8 January 2013

Abstract: Cyclic thermal exposure tests of infrared heating to 800 °C in 120 s followed by compressed air cooling to 150 °C in 60 s were performed for the laser deposited Ti60A (Ti5.54Al3.38Sn3.34Zr0.37Mo0.46Si) alloy. The effects of thermal exposure cycles on length of β phase, area fraction of α phase and microhardness of alloy were examined by OM, SEM and EDS. The results indicate that thermal exposure cycles have significant effects on length of β phase, area fraction of α phase and microhardness of the alloy. The original fine basket-weave β and 78.5% α transform to transient wedge-like β, finally leaving granular β and 97.6% coarsened α with the increased thermal exposure cycles. The formation mechanism of coarsened α and broken-up β microstructure is discussed. The alloy after 750 thermal exposure cycles has the maximum microhardness, 33.3% higher than that of the as-deposited alloy.
Key words: laser melting deposition; titanium alloy; cyclic thermal exposure; microstructure

1 Introduction

Near α titanium alloys have been extensively used in aero-engines as compressor disks and blades because they exhibit both excellent creep property of α alloys and high strength of $\alpha+\beta$ alloys [1]. Typical examples are Ti−Al−Sn−Zr−Mo−Si alloys, such as IMI834, IMI829, BT18Y, Ti-1100 and Ti60A alloy [2]. A near α high-temperature titanium alloy, Ti60A (Ti5.54Al3.38Sn3.34Zr0.37Mo 0.46Si), was developed in China to be used up to 600 °C for the compressor disks and blades in aero-engines [3]. Manufacturing of these critical titanium alloy components by the traditional wrought based processes involved a series of hot working steps [4], resulting in time consuming and high manufacturing cost. Laser melting deposition (LMD) manufacturing was a rapid solidification process based on layer-by-layer materials melting and deposition to fabricate fully dense near-net-shape metallic components [5−9]. Titanium alloy parts with dimensions up to 1730 mm×250 mm×230 mm and mass up to 50 kg per part could be successfully produced by LMD manufacturing [5]. Therefore, the ability to fabricate large near-net fully dense parts gave LMD an advantage to other techniques, especially for manufacturing aerospace components.

An important issue of near α titanium alloys was service reliability, which was greatly affected by microstructure evolution during severe temperature-fluctuating service process [10]. Like other near α titanium alloys, a certain amount of Al, Sn, Zr, Si and so on as the primary alloy elements were added to Ti60A alloy to enhance their heat-resistance [11]. However, the high heat-resistance was usually obtained at the cost of thermal stability loss. The main factors were surface oxidation and microstructural changes during long-term high temperature exposure [12−14]. GUAN et al [3] and JIA et al [15,16] reported that surface oxidation was the main reason for microstructural changes and the reduction in ductility during thermal exposure. In addition, the coarsening of the γ' precipitates was the key factor for the degradation of long-term thermal stability of CMSX-10 superalloy [17]. Till now, few studies have actually addressed the effect of thermal exposure on the microstructures of laser melting deposited Ti60A alloy. Furthermore, as for compressor components applied in the cyclic temperature-fluctuating service environment, cyclic thermal exposure is more reasonable than traditional constant temperature thermal exposure to reflect service reliability of the alloy.

Foundation item: Project (2010CB731705) supported by the National Basic Research Program of China
Corresponding author: Dong LIU; Tel: +86-10-82339691; E-mail: liudong.buaa@gmail.com
DOI: 10.1016/S1003-6326(13)62860-5

The objective of the current work is to investigate the microstructure evolution behavior of laser deposited Ti60A alloy as a function of thermal exposure cycles. Effect of thermal exposure cycles on length of β phase, area fraction of α phase and microhardness of the alloy is examined by OM, SEM and EDS. The formation mechanism of the broken-up β phase within α matrix during cyclic thermal exposure is discussed.

2 Experimental

2.1 Laser melting deposition of Ti60A alloy

Laser melting deposition (LMD) was a material additive rapid solidification near net-shaping technology controlled by a computer-aided design (CAD) model [18]. The high energy focused laser beam was employed to induce the melting pool during the scanning controlled by a CNC motion system. The alloy powders were injected into the laser focused zone and fully melted and rapidly solidified layer-upon-layer directly into near net-shape structure. Similar forming process of laser melting deposited plate sample was shown in Ref. [19] in detail.

The Ti60A alloy plate with dimensions of 250 mm×150 mm×30 mm was fabricated using a Rofin DC050 type 5 kW CO_2 LMD manufacturing system in an argon purged processing chamber with an oxygen volume fraction less than 70×10^{-6}. The LMD processing parameters were as follows: laser power 5 kW, beam diameter 5 mm, beam travel speed 500 mm/min, powder feed rate 600 g/h. After the LMD process, the material received a stress relieving treatment at 650 °C for 4 h, followed by air cooling. In this work, this state would be referred to as the "as-deposited" state.

2.2 Cyclic thermal exposure test

Chip-like specimens with dimensions of 40 mm× 12 mm×3 mm were machined from the laser deposited Ti60A plate. The cyclic thermal exposure (CTE) test was conducted in infrared heating & compressed air cooling device with 4 infrared lamps of 6 kW. The equipment power varied through the program adjustment to provide different quantities of heat automatically and accurately. Chip-like specimens are shown in Fig. 1. 800 °C was selected as the maximum CTE temperature to ensure service temperature of 600 °C in most service time, which was the general service temperature of most near α titanium alloys. The lowest temperature obtained via compressed air cooling was 150 °C. The average infrared heated area was 12 mm×12 mm×3 mm in the middle of the specimen. Each thermal exposure cycle consisted of infrared heating to 800 °C in 120 s followed by compressed air cooling to 150 °C in 60 s (Fig. 1(d)). The numbers of cyclic thermal exposures of 50, 250, 500 and 750, were referred to as TE50, TE250, TE500 and TE750, respectively.

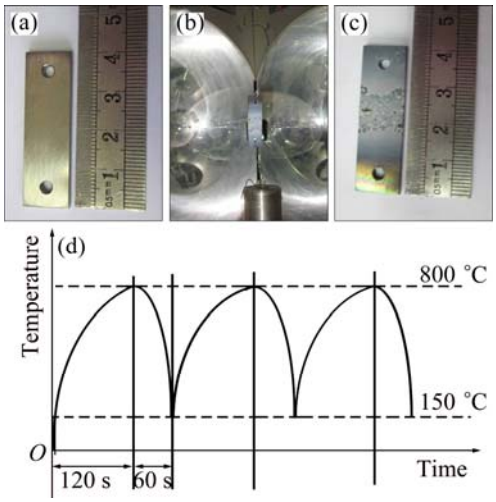

Fig. 1 Specimens of laser deposited Ti60A alloy before (a), during (b) and after (c) cyclic thermal exposure test, and illustration of cyclic thermal exposure (d)

2.3 Microstructure characterization

Metallographic specimens of laser deposited Ti60A alloy before and after CTE were prepared by mechanically grinding and etched by a solution of 1 mL HF, 6 mL HNO_3 and 143 mL H_2O. To investigate the depth of the surface oxidation penetration zone, 40 mm×3 mm section of the specimen was examined with optical microscope (OM). To avoid any effects from oxidation, the center microstructure of the 40 mm×3 mm section was examined by CamScan3400 scanning electron microscope (SEM) equipped with energy dispersive spectrometer (EDS). Quantitative measurements of the area fraction of α phase and the length of β phase were conducted on at least five micrographs with different magnifications for each specimen. Microhardness was measured using a HXZ−1000 Vickers tester with a test load of 4.9 N and a dwell time of 10 s.

3 Results and discussion

3.1 Microstructure of as-deposited Ti60A alloy

Microstructure of laser deposited Ti60A alloy is shown in Fig. 2. The α/β lamellar colony is formed through the solid state phase transformation from prior β phase during rapid cooling through the β-transus temperature in LMD process. The orientation of the colonies is largely related to the twelve variants of the Burger's relations. The α/β lamellae grows following the Burgers orientation relationship, $\{0001\}_\alpha//\{110\}_\beta//$, $\langle11\bar{2}0\rangle_\alpha//\langle111\rangle_\beta$ [20]. The alloy has a fine basket-weave microstructure with α lath spacing approximately 1.5−4.3 μm and β lamellar length with an average of 20 μm. The area fraction of α phase is approximately 78.5% (Fig. 2(b)).

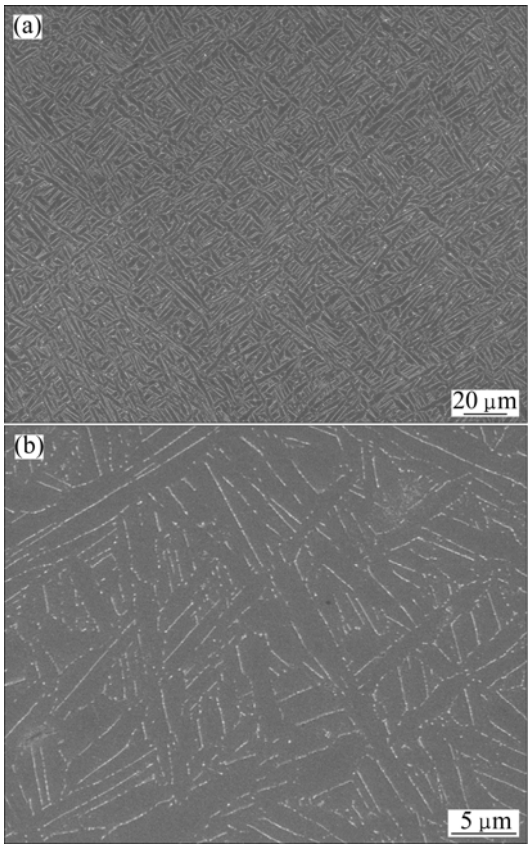

Fig. 2 SEM micrographs showing microstructure of as-deposited Ti60A alloy

3.2 Effect of cyclic thermal exposure on microstructure

The OM images of 40 mm×3 mm section of laser deposited Ti60A samples after different CTE tests are shown in Fig. 3. The dash line indicates the boundary of the degraded microstructure marked by zone *A* and pure *α* featureless zone marked by zone *B*. The average EDS results of oxygen content of zone *A* and the average depth of zone *B* are shown in Fig. 4. The average oxygen content of zone *A* (mass fraction, %) increases from 3.42% (TE50) to 7.02% (TE750). Similarly, the average depth of zone *B* increases from 40 μm (TE50) to 215 μm (TE750). It can be mainly attributed to more oxygen penetrating into the alloy, and oxygen element acts as one of the most important *α* phase stabilizing elements. Large pure *α* zone is developed with the increased thermal exposure cycles.

The enhanced oxygen penetration process can be mainly affected by the thermal stress accumulation with the increase in thermal exposure cycles. Although alloy atoms distribute uniformly, uphill chemical diffusion happens easily when stress gradient exists in the alloy [21].

$$D=kTB \quad (1)$$

$$V=BF \quad (2)$$

where *D* represents chemical diffusion rate, *k* represents diffusion constant, *T* represents temperature, *B* represents

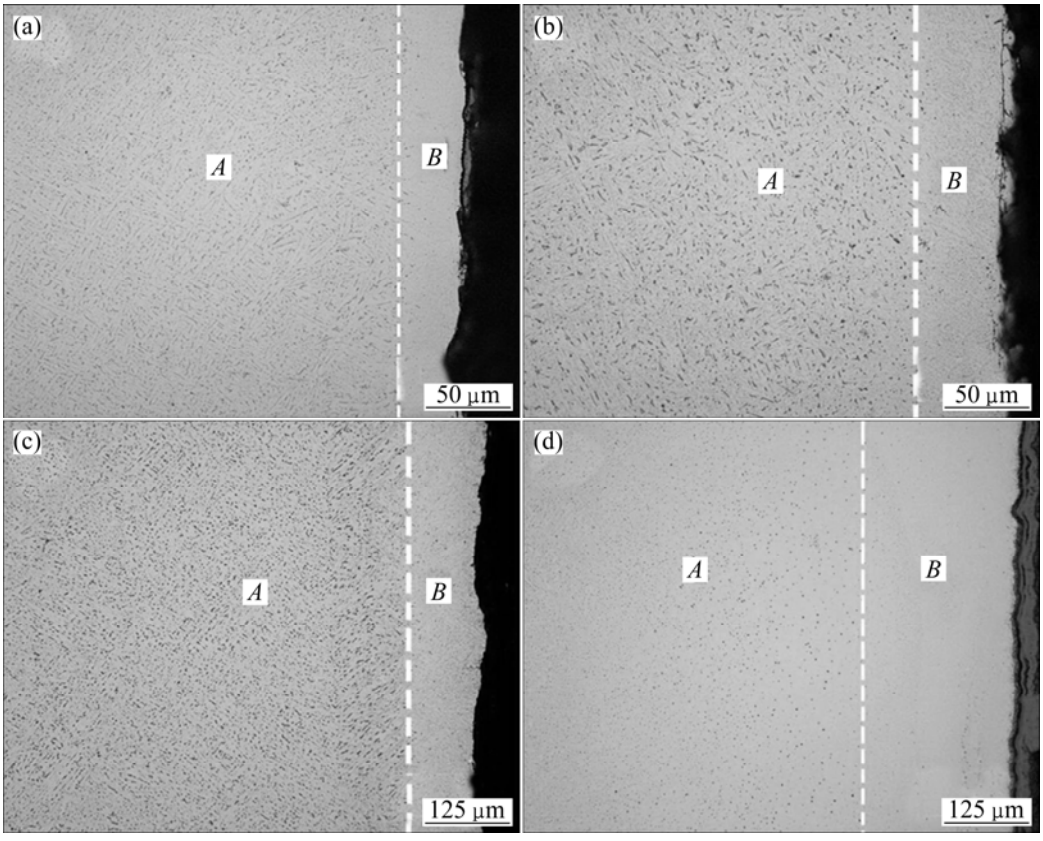

Fig. 3 OM micrographs showing 40 mm×3 mm section of laser deposited Ti60A alloy: (a) TE50; (b) TE250; (c) TE500; (d) TE750

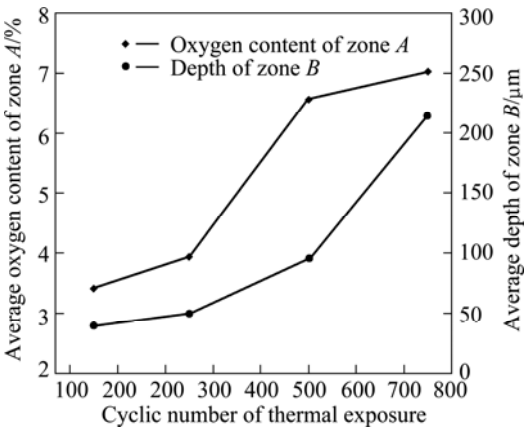

Fig. 4 Effect of thermal exposure cycles on average oxygen content of zone *A* and average depth of zone *B*

transfer rate, *V* represents atom diffusion rate and *F* represents value of stress.

Equations (1) and (2) illustrate that chemical diffusion rate (*D*) is determined by transfer rate (*B*) and temperature (*T*), and stress gradient (*F*) is the driving force for atomic diffusion rate (*V*). With the increasing thermal exposure cycles, stress gradient is accumulated in the laser deposited Ti60A alloy and enhances the atomic diffusion. Thus more oxygen atoms occupy the interstitial positions dissolving in α solid solution, resulting in the enhanced oxygen penetration process.

Microstructures of the laser deposited Ti60A alloy after cyclic thermal exposure are shown in Fig. 5. According to the Rosenberg's aluminum equivalent formula [Al]eq=[Al]+[Sn]/3+[Zr]/6+10(O+2N+C)≤9, the aluminum equivalent of laser deposited Ti60A alloy is 7.23, which is lower than the critical value of 9. This means that the microstructural changes during thermal exposure may not lead to the development of α_2 phase and silicides. Microstructure of TE50 changes little (Figs. 5(a) and (b)), compared with the as-deposited alloy (Fig. 2). Few β phases start to disperse, and some edges of the β phases coarsen slightly. It is notable that the original basket-weave microstructures become so dissociated that cannot be distinguished any more from TE250 to TE750 (Figs. 5(c)−(h)). The coarsened wedge-like β phase of TE250 and TE500 are the intermediate morphology (Figs. 5(d) and (f)). Finally, few granular β phase and most α matrix occur in the alloy (Figs. 5(g) and (h)). Meanwhile, the length of β phase decreases from 20 to 3 μm and the area fraction of α phase increases from 78.5% to 97.6% with the increased thermal exposure cycles (Fig. 6). There is a microstructure evolution tendency that the as-deposited lamellar β phase breaks to granular β phase, and higher area fraction of stabilized α phase occurs. The possible tendency of the final microstructure after numerous thermal exposure cycles is the disappearing of all β phases and the development of all α phases.

3.3 Formation mechanism of unique microstructure of broken-up β phase in α matrix

Schematic diagram of the formation of the special broken-up β phase and coarsened α microstructure during cyclic thermal exposure is shown in Fig. 7. It is essentially attributed to β phase coarsening and dissolving interactive process during thermal exposure cycle. The oxygen content of TE250 is 3.92%, while the oxygen contents of TE500 and TE750 increase to 6.56% and 7.02%, respectively (Fig. 4). In the previous 250 thermal exposure cycles, the oxygen penetration is insignificant, so every thermal exposure cycle is dominant. Each thermal cycle contains 120 s up to high temperatures while 60 s down to low temperatures (Fig. 1(d)), the time of α transforming to β process is longer than β transforming to α, so the β phase coarsening plays a leading role. Different phase boundary morphologies result from different interfacial structures and energies between β phase and different parts of α laths [22,23]. Some active α/β phase boundaries dissolved and released β stabilizing elements. The immigration of α/β phase boundaries leads to the formation of broken and coarsened lamellar β phase during previous 250 cycles.

The oxygen penetration process is enhanced with the increased thermal exposure cycles (Fig. 4) and oxygen as one of the most significant α stabilizing elements is helpful to form stabilized α phase. So, β dissolving process is dominant and coarsened α phase is developed in the later 250 to 750 thermal exposure cycles. It is acknowledged that the specific surface energy of granular β phase is in more thermodynamic steady state than the wedge-like β phase. Thus, the wedge-like β phase is the intermediate transient morphology, and the smaller size of broken-up β phase and edges of wedge-like β phase disappear together, leaving a small amount of granular β phase and coarsened α phase alone.

3.4 Effect of cyclic thermal exposure on microhardness

The influence of cyclic thermal exposure on microhardness of the laser deposited Ti60A alloy is shown in Fig. 8. The microhardness values of TE50 and TE250 increase slightly. While, it is notable that the hardness of TE500 increases by 18.7% compared with the as-deposited one. The microhardness curve displays a linear increase feature from TE250 to TE750. There is a hardness peak for TE750, which is 33.3% higher than that of the as-deposited one.

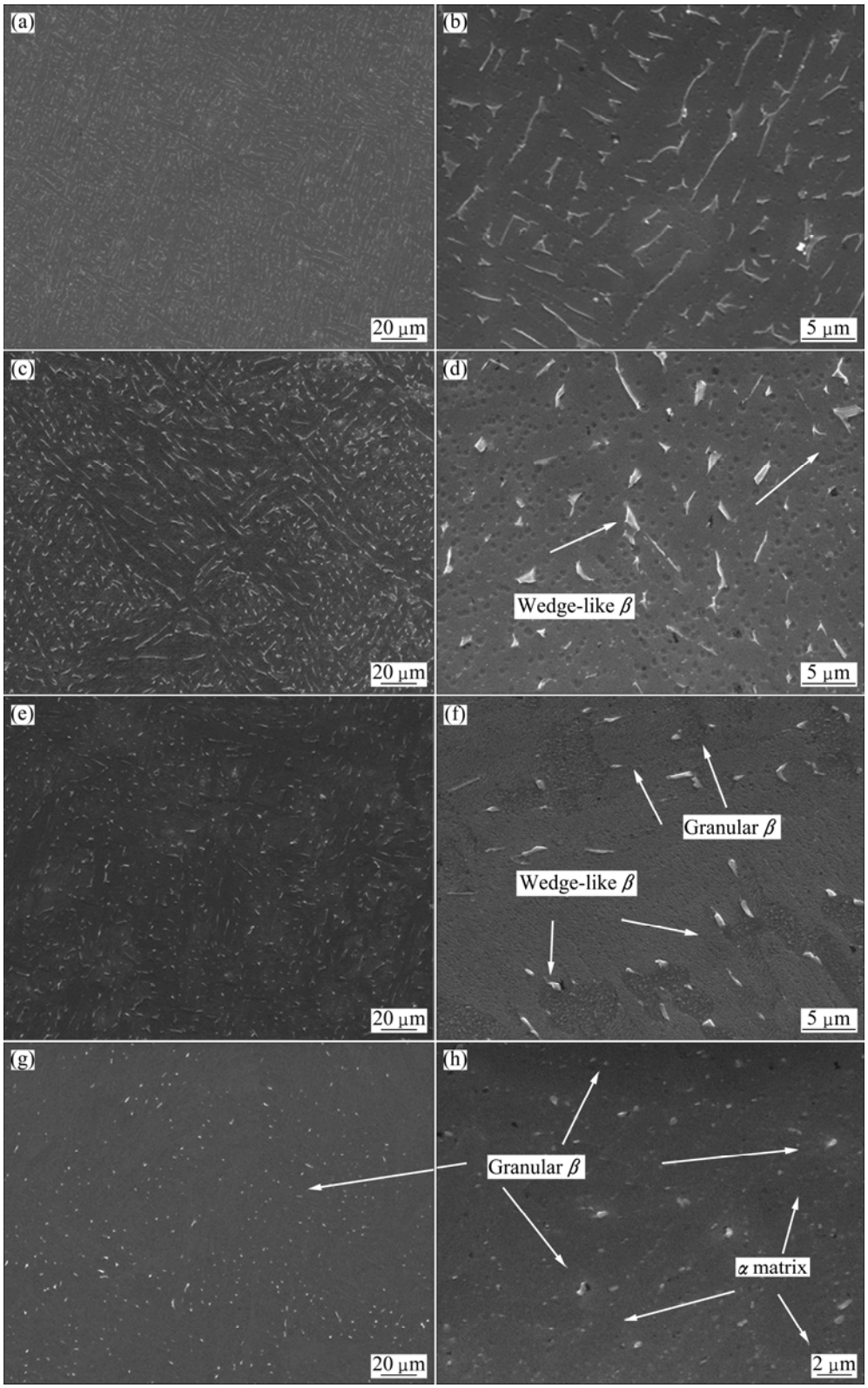

Fig. 5 SEM micrographs showing microstructures of laser deposited Ti60A alloy: (a), (b) TE50; (c), (d) TE250; (e), (f) TE500; (g), (h) TE750

It can be seen explicitly that both area fraction of α phase and length of β phase of TE50 change little (Fig. 6), and the same microstructure is nearly the same as the as-deposited one, so the hardness of TE50 increases slightly. Earlier investigations demonstrated oxygen diffusion during high service temperature inducing

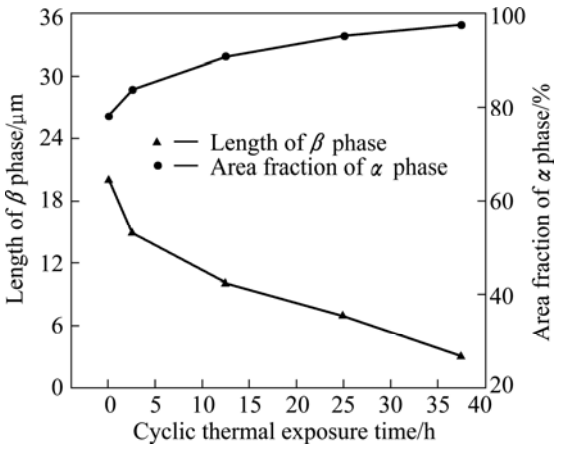

Fig. 6 Effects of thermal exposure cycles on length of β phase and area fraction of α phase

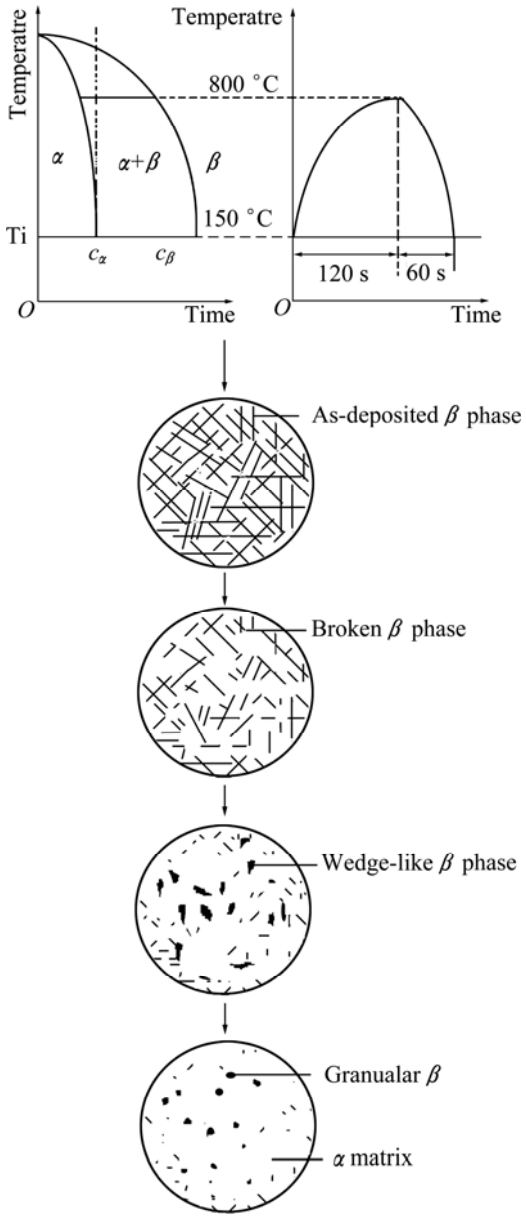

Fig. 7 Schematic diagram of formation of broken-up β and coarsened α during cyclic thermal exposure

alloy hardening. Oxygen diffusion hardening treatment increased the hardness of Ti−6Al−7Nb alloy gradually [24]. Moreover, it is presented that high temperature exposure leads to the increase in the strength of Ti−6Al−4V alloy [25]. These explanations of alloy hardening are similar with our results. In the present study, the oxygen penetration process can be enhanced with the increasing thermal exposure cycles from 250 to 750 (Fig. 4). The alloy hardening is mainly attributed to interstitial oxygen atoms solid-solution strengthening effect induced by enhanced oxygen penetration process during cyclic thermal exposure. This greatly explains the linear increase of microhardness curve from 250 to 750 thermal exposure cycles, with a hardness peak for TE750 (Fig. 8).

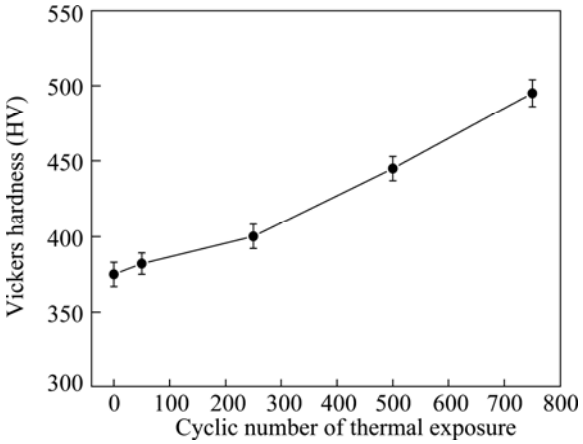

Fig. 8 Microhardness of laser deposited Ti60A alloy as function of thermal exposure cycle

According to the aforementioned results of microhardness and microstructure evolution of the laser deposited Ti60A alloy during cyclic thermal exposure, it can be concluded that the whole hardened and brittle α phases are the production of near α titanium alloys after a long-term temperature fluctuating service process. Further investigation of finite element analysis of temperatures and cyclic thermal stresses is necessary to examine and control the cyclic thermal exposure damage accurately.

4 Conclusions

1) The microstructure of laser deposited Ti60A alloy evolves from the original fine basket-weave β phase and 78.5% α phase to transient wedge-like β phase, finally leaving a small amount of granular β phase in 97.6% α matrix with the increased thermal exposure cycles.

2) The microstructure of broken-up β phase and coarsened α phase is attributed to the special thermal cycles in the former 250 cycles. Subsequently, it is

mainly produced by oxygen penetration process, which is promoted by cyclic thermal stress accumulation.

3) Microhardness of the alloy presents linear increase after 250 thermal exposure cycles. The alloy after 750 thermal exposure cycles has the highest microhardness, 33.3% higher than that of the as-deposited one. They are mainly attributed to interstitial oxygen atoms solid-solution strengthening induced by enhanced oxygen penetration during cyclic thermal exposure.

References

[1] LEYENS C, PETERS M. Titanium and titanium alloys [M]. Zhen-hua CHEN, et al. Beijing: Chemical Industry Press, 2005: 6−10. (in Chinese)

[2] BOYER K, WELSCH G, COLLING E W. Materials properties handbook: Titanium alloys [M]. Materials Park (OH): ASM International, 1994: 431−434.

[3] GUAN Shao-xuan, KANG Qiang, WANG Qing-jiang, LIU Yu-yin, LI Dong. Influence of long-term thermal exposure on the tensile properties of a high-temperature titanium alloy Ti-55 [J]. Materials Science and Engineering A, 1998, 243: 182−185.

[4] WEISS I, SRINIVASAN R, BANIA P J, EYLON D, SEMIATIN S L. Advances in the science and technology of titanium alloy processing [M]. Warrendale, PA: TMS, 1997: 72−73.

[5] WANG Hua-ming, ZHANG Ling-yun, LI An, CAI Liang-xu, TANG Hai-bo, LU Xu-dong. Progress on rapid solidification laser processing for advanced materials and components [J]. World Science Technology R&D, 2004, 26(3): 27−31. (in Chinese)

[6] GAO Fei, WANG Hua-ming. Abrasive wear property of laser melting/deposited Ti_2Ni/TiNi intermetallic alloy [J]. Transactions of Nonferrous Metals Society of China, 2007, 17: 1358−1362.

[7] LIU Dong, ZHANG Shu-quan, LI An, WANG Hua-ming. Microstructure and tensile properties of laser melting deposited TiC/TA15 titanium matrix composites [J]. Journal of Alloys and Compound, 2009, 485(1−2): 156−162.

[8] LU Ying, TANG Hai-bo, FANG Yan-li, LIU Dong, WANG Hua-ming. Microstructure evolution of sub-critical annealed laser deposited Ti−6Al−4V alloy [J]. Materials & Design, 2012, 37: 56−63.

[9] LIU Jian-di, ZHANG Shu-quan, WANG Hua-ming. Microstructure and wear resistance of laser cladding WC particles reinforced composite coating [J]. The Chinese Journal of Nonferrous Metals, 2012, 22(9): 2600−2607. (in Chinese)

[10] POORGANJI B, YAMAGUCHI M, ITSUMI Y, MATSUMOTO K, TANAKA T, ASA Y, MIYAMOTO G, FURUHARA T. Microstructure evolution during deformation of a near-α titanium alloy with different initial structures in the two-phase region [J]. Scripta Materialia, 2009, 61(4): 419−422.

[11] ZHANG Shang-zhou, WANG Bo, LIU Zi-quan, GAO Yuan, YANG Rui. Effect of carbon on microstructures and mechanical properties of Ti60 high temperature titanium alloy [J]. Chinese Journal of Material Research, 2007, 21: 433−438. (in Chinese)

[12] SRINADH K V S, SINGH V. Oxidation behavior of the near α titanium alloy IMI834 [J]. Bulletin Material Science, 2004, 27: 347−354.

[13] CHEN Hui-qin, CAO Chun-xiao. Characterization of hot deformation microstructures of alpha—beta titanium alloy with equiaxed structure [J]. Transactions of Nonferrous Metals Society of China, 2012, 22: 503−509.

[14] JIA Wei-ju, ZENG Wei-dong, ZHOU Yi-gang, LIU Jian-rong, WANG Qing-jiang. High temperature deformation behavior of Ti60 titanium alloy [J]. Materials Science and Engineering A, 2011, 528: 4068−4074.

[15] JIA Wei-ju, ZENG Wei-dong, ZHOU Yi-gang, LIU Jian-rong, WANG Qing-jiang. Influence of thermal exposure on the tensile properties and microstructures of Ti60 titanium alloy [J]. Materials Science and Engineering A, 2011, 530: 511−518.

[16] JIA Wei-ju, ZENG Wei-dong, YU Han-qing, ZHOU Yi-gang. Effect of thermal exposure on properties and fracture behaviors of Ti60 alloy [J]. The Chinese Journal of Nonferrous Metals, 2009, 19(6): 1032−1037. (in Chinese)

[17] ACHARYA M V, FUCHS G E. The effect of long-term thermal exposures on the microstructure and properties of CMSX-10 single crystal Ni-base superalloys [J]. Materials Science and Engineering A, 2004, 381: 143−153.

[18] WANG Hua-ming, ZHANG Ling-yun, LI An, CAI Liang-xu, TANG Hai-bo. Rapid solidification laser processing and forming of advanced aeronautical metallic materials [J]. Journal of University of Aeronautics and Astronautics, 2004, 30(10): 962−967. (in Chinese)

[19] WANG Yu-dai, TANG Hai-bo, FANG Yan-li, WANG Hua-ming. Microstructure and mechanical properties of laser melting deposited 1Cr12Ni2WMoVNb steel [J]. Materials Science and Engineering A, 2010, 527: 4804−4809.

[20] HE Rui-jun, WANG Hua-ming. Fatigue crack nucleation and growth behaviors of laser melting deposited Ti−6Al−2Zr−Mo−V [J]. Materals Science and Engineering A, 2010, 527(7−8): 1933−1937.

[21] HU Geng-xiang, CAI Xun. Foundation of material science [M]. Shanghai: Shanghai Jiao Tong University Press, 2000: 130−140. (in Chinese)

[22] YANG Yi, XU Feng, HUANG Ai-jun, LI Ge-ping. Evolution of microstructure of full lamellar titanium alloy BT18Y solutionized at $\alpha+\beta$ phase field [J]. Acta Metallurgica Sinica, 2005, 41(7): 713−720. (in Chinese)

[23] MIRONOV S, MURZINOVA M, ZHEREBTSOV S, SALISHCHEV G A, SEMIATIN S L. Microstructure evolution during warm working of Ti−6Al−4V with a colony-α microstructure [J]. Acta Materialia, 2009, 57(8): 2470−2481.

[24] STREICHER R M, WEBER H, SCHÖN R, SEMLITSCH M. New surface modification for Ti−6Al−7Nb alloy [J]. Oxygen Diffusion Hardening (ODH). Biomaterials, 1991, 12(2): 125−129.

[25] ROSEN A, ROTTEM A. The effect of high temperature exposure on the creep resistance of Ti−6Al−4V alloy [J]. Materials Science and Engineering, 1976, 22: 23−29.

激光沉积 Ti60A 钛合金的循环热暴露显微组织演变

张阿莉，刘 栋，汤海波，王华明

北京航空航天大学 大型整体金属构件激光直接制造教育部工程研究中心，北京 100191

摘 要：在激光沉积 Ti60A 合金片状试样(40 mm×12 mm×3 mm)上进行一系列的循环热暴露模拟实验，每个循环包括红外加热 120 s 至最高 800 °C，随后压缩空冷 60 s 至最低 150 °C。采用 OM、SEM 及 EDS 分析了合金 α 相体积分数和 β 相长度，并测试其显微硬度随热暴露循环次数的变化。结果表明，随着热暴露循环次数的增加，激光沉积 Ti60A 合金从初始的网篮状 β 相和体积分数为 78.5%的 α 相逐渐向楔形 β 相和粗大 α 相过渡，750 次循环后转变为极少量颗粒状 β 相和体积分数为 97.6%的大块 α 组织。讨论了特殊粗大 α 和破碎 β 组织的形成机理。经 750 次热暴露循环后的合金最硬，其显微硬度比沉积态的高 33.3%。

关键词：激光熔化沉积；钛合金；循环热暴露；显微组织

(Edited by Hua YANG)